An electrolyte electroreflectance study of FeS_2

1993 J. Phys.: Condens. Matter 5 7827

(http://iopscience.iop.org/0953-8984/5/42/005)

J. Phys.: Condens. Matter 5 (1993) 7827–7836. Printed in the UK

An electrolyte electroreflectance study of FeS_2

Y S Huang, J K Huang and M Y Tsay
Department of Electronic Engineering, National Taiwan Institute of Technology, Taipei, Taiwan 106, Republic of China

Received 5 May 1993, in final form 14 June 1993

Abstract. We report an electrolyte electroreflectance (EER) study of synthetic pyrite FeS_2 single crystals in the energy range 1–6 eV. The EER spectrum exhibits derivative-like structures in the vicinity of the interband transitions. The transition energies are determined accurately and a probable energy band structure near the Fermi level is constructed. It is proposed that FeS_2 has a completely filled 3d t_{2g} band occupied by six electrons in the low-spin configuration, separated from empty S 3p σ^* and Fe 3d e_g^* bands, and that the bottom of the conduction band corresponds to the S 3p σ^* antibonding states.

1. Introduction

FeS_2 crystallizing in the pyrite structure, known as 'fool's gold', is the most abundant of all sulphide minerals. Electrical measurements show a semiconducting behaviour. Recently it has attracted great interest because of its possible application as a useful material for solar energy applications [1, 2], as a depolarized anode for hydrogen production [3] and as a cathode in high-energy-density batteries [4, 5]. Its physical [6] and chemical [7] properties have been widely studied. However, there are disagreements between various investigators concerning the fundamental properties of FeS_2. For example, there has been considerable controversy as to the value of the energy gap E_g for FeS_2 reported in the literature [8–13]. It is to be noted that most of the samples studied have been collected from coal mines and thus the samples will have different levels of impurities and different crystal qualities. These differences will make the comparison difficult and hence it is desirable to carry out the basic property studies on synthetic samples with a controlled level of impurities.

The energy band structure is one of the most important factors in determining the solid-state properties of a material. The electrolyte electroreflectance (EER) technique has proved to be a very powerful tool in the study of the band structure of semiconductors [14, 15]. It possesses the advantage of providing a spectrum with sharp features at precise energies, in contrast with the weak and poorly resolved corresponding features in the unmodulated spectra. Macfarlane *et al* [16] reported wavelength modulation reflectance spectra of FeS_2, covering a limited range 2–5.5 eV, and no detailed analysis of the spectrum was attempted. Recently, Salvador *et al* [17] reported an EER study on n-FeS_2 in contact with the I^-–I_n^- redox couple in the energy range between 2.06 and 4.13 eV. The bias-dependent study of the EER feature centred at about 3.13 eV was used to determine the flat-band potential of the pyrite–electrolyte system. In this report we present the EER spectrum of a synthetic FeS_2 single crystal in the range 1–6 eV. Derivative-like features are observed in the vicinity of the interband transitions. By comparing our results with recent band-structure and density-of-states calculations [18–20] as well as past experimental studies of FeS_2 [9, 12, 20–24] and RuS_2 [25, 26], several interband transitions are identified. Details of these results are presented and discussed in this paper.

0953-8984/93/427827+10$07.50

2. Experimental details

2.1. Preparation and properties of FeS_2 crystals

Single crystals of FeS_2 with mirror-like surfaces have been grown by an 'oscillating chemical vapour transport method' [27], using ICl_3 as the transport agent. The lattice parameters were determined by x-ray powder diffraction analysis, and the pyrite crystal structure has been confirmed. The largest dimensions of a single crystal as grown were about 5 mm × 5 mm × 5 mm. The (100) face appears to be the predominant growth face. Electrical resistivity and Hall effect measurements have revealed p-type semiconducting behaviour. At room temperature, the carrier concentrations are between 6×10^{15} and 7×10^{16} cm^{-3}, and the mobilities between 50 and 200 $cm^2\ V^{-1}\ s^{-1}$. From electron paramagnetic resonance studies [28], Cr^{3+} and Ni^{2+} ions were detected as impurities in these single crystals. The measured values of the mobilities were very high for a p-type pyrite. This might be due to a compensation effect induced by the presence of Cr^{3+} and Ni^{2+} ions. The energy gap was determined from the photoconductive spectral response by the Moss [29] rule, and the room-temperature indirect energy gap was found to be 0.83 eV [30].

2.2. EER measurements

Although the EER method has been described extensively in the literature [14, 15], the experimental set-up used in our present investigations incorporates a number of modifications to improve accuracy of measurement, as well as faster data acquisition and processing. The details of the present experimental set-up have been described elsewhere [31]. The detector response to the DC component of the reflected light is kept constant by either an electric servomechanism or a neutral density filter so that the AC reflectance is a direct measure of $\Delta R/R$, the differential reflectivity. Scans of $\Delta R/R$ versus wavelength are obtained using a 0.25 m Photon Technology International (PTI) grating monochromator together with an Osram 150 W xenon arc lamp as a monochromatic light source. Phase-sensitive detection is used to measure the differential reflectivity.

Prior to the measurements, the crystals were cut into thin slabs with a diamond saw parallel to the (100) face. The as-grown (100) faces were then etched in an HNO_3–HF–CH_3COOH solution (HNO_3:HF:CH_3COOH = 2:1:1) and rinsed with CH_3CH_2OH. The FeS_2 electrodes were prepared by passing a copper wire through a glass tube and soldering the free end to one end of a copper plate. The cut crystal was cemented to the copper plate with silver conducting paint. The wire and plate were then insulated with epoxy cement, leaving the (100) face exposed to the electrolyte, a 1 N H_2SO_4 aqueous solution. The counter-electrode was a 5 cm^2 platinum plate. To verify that measurements were performed in the low-field regime, EER was performed at $V_{DC} = 0$ V versus Pt with various AC modulation voltages. The results indicate that the lineshape remains invariant for $V_{AC} \leqslant 1 V_{p-p}$ and the amplitude of $\Delta R/R$ varies linearly with modulation voltage. The dependence of the EER spectra on the DC bias voltage was also checked. The amplitude and lineshape of EER features remained constant at different bias voltages. Subsequently a 200 Hz square wave was used to modulate the electric field with an amplitude 0.6 V_{p-p} at $V_{DC} = 0$ V versus Pt.

3. Results and discussion

EER measurements were carried out on five samples from different growth batches. All the five samples exhibited a similar spectral response. The typical EER spectrum of FeS_2

at room temperature in the range 1–6 eV is shown in figure 1. Derivative-like structures are apparent in the vicinity of interband transitions. These features are much broader than those of the III–V and II–VI semiconductors. This might correspond to the relatively flat nature of the bands near the Fermi level reported by Bullett [20]. The large differences between the amplitudes of the EER features indicate the different transition probabilities of the various transitions. Comparing the amplitude of these features might help us to make the correct assignment of the transitions. By fitting the EER spectrum with the Aspnes [32] third-derivative lineshape expression

$$\frac{\Delta R}{R} = \mathrm{Re}\left(\sum_{j=1}^{n} \frac{A_j \exp(\mathrm{i}\Theta_j)}{(E - E_j + \mathrm{i}\Gamma_j)^{2.5}}\right) \tag{1}$$

where E_j is the interband transition energy, A_j the amplitude, Θ_j the phase factor and Γ_j the broadening parameter, we can determine the position of the interband transitions to an accuracy better than 5 meV. The values of E_j obtained from equation (1) are indicated by arrows in figure 1. Table 1 shows the energy positions of interband transitions obtained from the EER spectrum and our assigment of the interband transitions.

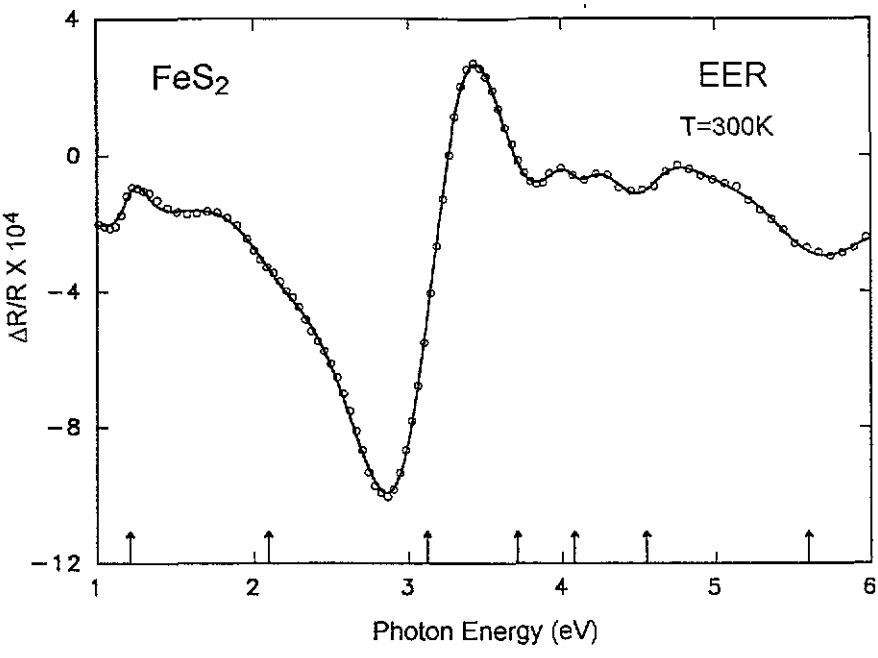

Figure 1. The EER spectrum (○) of FeS_2 at 300 K in the range 1–6 eV: ——, least-squares fits to the third-derivative functional form. The interband transition energies obtained are indicated by arrows.

FeS_2 is of the cubic pyrite structure. The space group is the cubic T_h^6 ($Pa3$), and there are four molecular units in a unit cell with $a = 5.407$ Å. The site symmetry at Fe is $\bar{3}$ and that at S is 3. The Fe–S_6 octahedron is not regular. Each S atom is coordinated with three Fe atoms at the base of a pyramid, and to an S atom at the apex of the pyramid. Figure 2 depicts the arrangement of the atoms in FeS_2 crystals, where each Fe^{2+} ion is surrounded

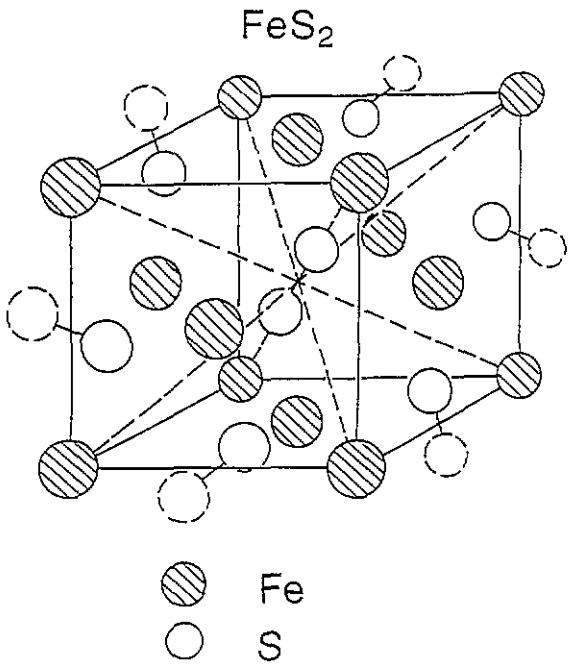

Figure 2. A drawing showing the arrangements of the atoms in a unit cell of FeS_2.

Table 1. Energy positions of various features observed in the EER spectrum of FeS_2 (see figure 1) and our assignment of the interband transitions.

FeS_2 feature (eV)	Assignment of interband transitions
1.22	Fe 3d $t_{2g} \rightarrow$ S 3p σ^*
2.09	Fe 3d $t_{2g} \rightarrow$ S 3p σ^*
3.12	Fe 3d $t_{2g} \rightarrow$ Fe 3d e_g^* + S 3p σ^*
3.71	Fe 3d $t_{2g} \rightarrow$ Fe 3d e_g^* + S 3p σ^*
4.08	S 3p $\rightarrow$ Fe 3d e_g^* + S 3p σ^*
4.55	S 3p $\rightarrow$ Fe 3d e_g^* + S 3p σ^*
5.60	S 3p $\rightarrow$ Fe 3d e_g^* + S 3p σ^*

by six S_2^{2-} molecules with the site symmetry represented by S_6. The octahedral component of the ligand field causes Fe 3d levels to be split into triply degenerate t_{2g} and doubly degenerate e_g components (see, e.g., [33]). The t_{2g} and e_g degeneracies are removed by the strong octahedral crystal field of the S_2^{2-} ions. The t_{2g} orbitals orient themselves away from the Fe–S bonding directions and are essentially non-bonding. The e_g orbitals, on the other hand, orient themselves along the Fe–S bonding directions and hybridize with the S 3p levels. This hybridization occurs in such a way as to preserve the level structure of the S 3p bands of the hypothetical S_2^{2-} material. The antibonding Fe 3d e_g^*–S 3p σ^* hybrid states form conduction bands. In general, the conduction bands are strongly hybridized with each other.

In order to analyse our experimental results, we have made use of recent theoretical work [18–20] as well as past experimental studies of FeS_2 [9, 12, 20–24] and RuS_2 [25, 26]. Information about the top of the valence band of FeS_2 and its lower levels was obtained by Ohsawa *et al* [21] using x-ray photoelectron spectroscopy (XPS), and by Li *et al* [22] using ultraviolet photoelectron spectroscopy. The latter results gave information on the electronic structures of mostly the top of the valence band. The shape of the ultraviolet photoelectron spectrum was similar to that of the XPS curve. A very sharp XPS peak with an FWHM of 1.3 eV was observed near 0.9 eV below the Fermi level. A similar peak was also found in the ultraviolet photoelectron spectrum. Self-consistent field Xα cluster calculations indicate that this narrow localized non-bonding level consists of Fe 3d-like t_{2g} states. A broader peak near 4 eV was attributed to the S 3p-valence band.

Table 2 is a summary of the reflectance structures and assignments for FeS_2 from various investigators [9, 12, 23, 24]. The pioneering work of Bither *et al* [9] on optical reflectivity measurement of FeS_2 had a great impact on the studies of the physical problems of the material. They measured a near-normal-incidence reflectivity spectrum from as-grown crystal faces of FeS_2 and gave merely tentative assignments to the spectrum, since only qualitative molecular orbital diagrams were available at the time. The absorption edge E_1 of the lowest-energy peak corresponds to the onset of the Fe 3d t_{2g}–e_g^* transition. They estimated the energy position of the S 3p-conduction band to be at least 2.5 eV above the e_g^* level, thus attributing the E_2, E_3 and E_4 peaks also to Fe 3d t_{2g}–e_g^* transitions. Schlegel and Wachter [12] reported the reflectivity spectrum of FeS_2 between 0.03 and 12 eV. They related the peak at about 2 eV to Fe 3d intraband transitions from 3d t_{2g} into the antibonding e_g^* state and the structure at higher energies from 3 eV to at least 8.5 eV to the interband transitions from the state with mostly S 3p character to the e_g^* state. They paid special attention to a constant splitting of 0.6 eV of all maxima in the energy range between 1 and 8.5 eV and attributed this splitting to a splitting of the final state e_g^* due to the S_6 site symmetry of the Fe ions. Suga *et al* [23] measured the VUV reflectivity spectrum of FeS_2 from 4 to 30 eV using synchrotron radiation. For low-energy regions they assigned the peaks at 1.6 and 4.0 eV to the transitions from the rather narrow Fe 3d t_{2g} bands to the Fe 3d e_g^* and S 3p σ^* bands. The structures at 5.1 and 5.9 eV were interpreted as being due to the excitation from the S 3p-valence band to Fe 3d e_g^* and S 3p σ^* bands. Sato [24] reported the reflectivity spectrum of FeS_2 for photon energies between 0.2 and 4.4 eV. He assigned the peak at around 1.3 eV as the band-to-band transition from the occupied Fe 3d t_{2g} states to the unoccupied 3d e_g^* states and the peak at around 3 eV as a transition from the t_{2g} band to the upper part of the e_g^* band, in which the p-like character dominates.

Shown in figure 3 is the total density of states (DOS) and the partial DOS for FeS_2 from recent theoretical calculation by Folkerts *et al* [18]. The effect of the crystal-field splittings of the 3d electron states into t_{2g} and e_g bands is indicated. The S 3s partial DOS consists mainly of two discrete bands arising from bonding and antibonding orbitals in the S_2 pairs. The next-higher group of bands is labelled S 3p–Fe 3d e_g. One sixth of the S 3p bands associated with 3p σ^* antibonding orbitals of the S_2 pairs lie above E_F, giving a peak in the DOS at 3.4 eV above the top of the valence band. The first 2.7 eV of the unoccupied DOS are denoted as antibonding S 3p σ^*–Fe 3d e_g^* hybrid states. Between the S 3p σ^* bands and the next conduction band is a gap of 2.0 eV. The conduction band which starts at 5.9 eV is of mixed S 3d–Fe 4sp character.

The wavelength-modulated reflectivity (WMR) measurements of FeS_2 were performed by Macfarlane *et al* [16] in the range 2–5.5 eV. Their WMR spectrum also shows derivative-like features at around 2.6, 3.2, 3.8, 4.1, 4.6 and 5.1 eV but no detailed analysis was made. While the spectral positions of some of the features of the WMR spectrum are comparable

Table 2. The summary of the reflectance structures and assignments for FeS_2 from various investigators [9, 12, 23, 24].

FeS_2 feature (eV)	Assignment of interband transitions
1.46 (E_1) [9]	Fe 3d $t_{2g} \rightarrow$ Fe 3d e_g^*
1.75 (E_2) [9]	Fe 3d $t_{2g} \rightarrow$ Fe 3d e_g^*
2.45 (E_3) [9]	Fe 3d $t_{2g} \rightarrow$ Fe 3d e_g^*
2.80 (E_4) [9]	Fe 3d $t_{2g} \rightarrow$ Fe 3d e_g^*
1.7 [12]	Fe 3d $t_{2g} \rightarrow$ Fe 3d e_g^*
2.3 [12]	Fe 3d $t_{2g} \rightarrow$ Fe 3d e_g^*
3.8 [12]	S 3p $\rightarrow$ Fe 3d e_g^*
4.45 [12]	S 3p $\rightarrow$ Fe 3d e_g^*
5.2 [12]	S 3p $\rightarrow$ Fe 3d e_g^*
5.85 [12]	S 3p $\rightarrow$ Fe 3d e_g^*
1.6 [23]	Fe 3d $t_{2g} \rightarrow$ Fe 3d $e_g^* +$ S 3p σ^*
4.0 [23]	Fe 3d $t_{2g} \rightarrow$ Fe 3d $e_g^* +$ S 3p σ^*
5.1 [23]	S 3p $t_{2g} \rightarrow$ Fe 3d $e_g^* +$ S 3p σ^*
5.9 [23]	S 3p $t_{2g} \rightarrow$ Fe 3d $e_g^* +$ S 3p σ^*
1.3 (A) [24]	Fe 3d $t_{2g} \rightarrow$ Fe 3d e_g^*
3.0 (B) [24]	Fe 3d $t_{2g} \rightarrow$ Fe 3d $e_g^* +$ S 3p σ^*

with those of our EER spectrum, there are considerable differences between the relative amplitudes displayed by the EER spectrum and those displayed by the WMR spectrum. The EER feature centred at about 3.1 eV is dominant compared with all the other features which are comparatively weak. In the WMR spectrum at 293 K, the 3.8 eV feature is larger than the others but is not so dominant, and the other features are clearly discernible. These differences might arise because of the different modulation mechanisms of the WMR and EER. The WMR measurement system can generate intrinsic structures which are not easy to eliminate [15].

On comparison of our results with previous reports and those discussed above, it is possible to associate the features of the EER spectrum with the appropriate interband transitions. Because of the small amplitude which might correspond to the low transition probabilities, we can relate the features at 1.22 and 2.09 eV to the transitions from the Fe 3d t_{2g} non-bonding states to the antibonding S 3p σ^* states. The amplitudes of the features at 3.12 and 3.71 eV are about one order larger than those of other features. Following the assignment by Sato [24], we attribute the origin of these two features to the transitions from the Fe 3d t_{2g} non-bonding states to the antibonding Fe 3d e_g^*–S 3p σ^* hybrid states. The structures at higher energies from 4 to 6 eV are mainly due to interband transitions from states of largely S 3p character to Fe 3d e_g^*–S 3p σ^* hybrid states.

According to the previous optical absorption investigations [12, 13], the fundamental band gap of FeS_2 is indirect. Recently Holzwarth *et al* [26] reported the band-structure calculation of the related material, RuS_2, and the results show that the bottom of the conduction band is the S 3p σ^* antibonding states. Folkerts *et al* [18] reported the bremsstrahlung isochromat spectrum of FeS_2 which is the first direct experimental evidence for a sharp antibonding p-like state above the Fermi level. By adopting their results we are

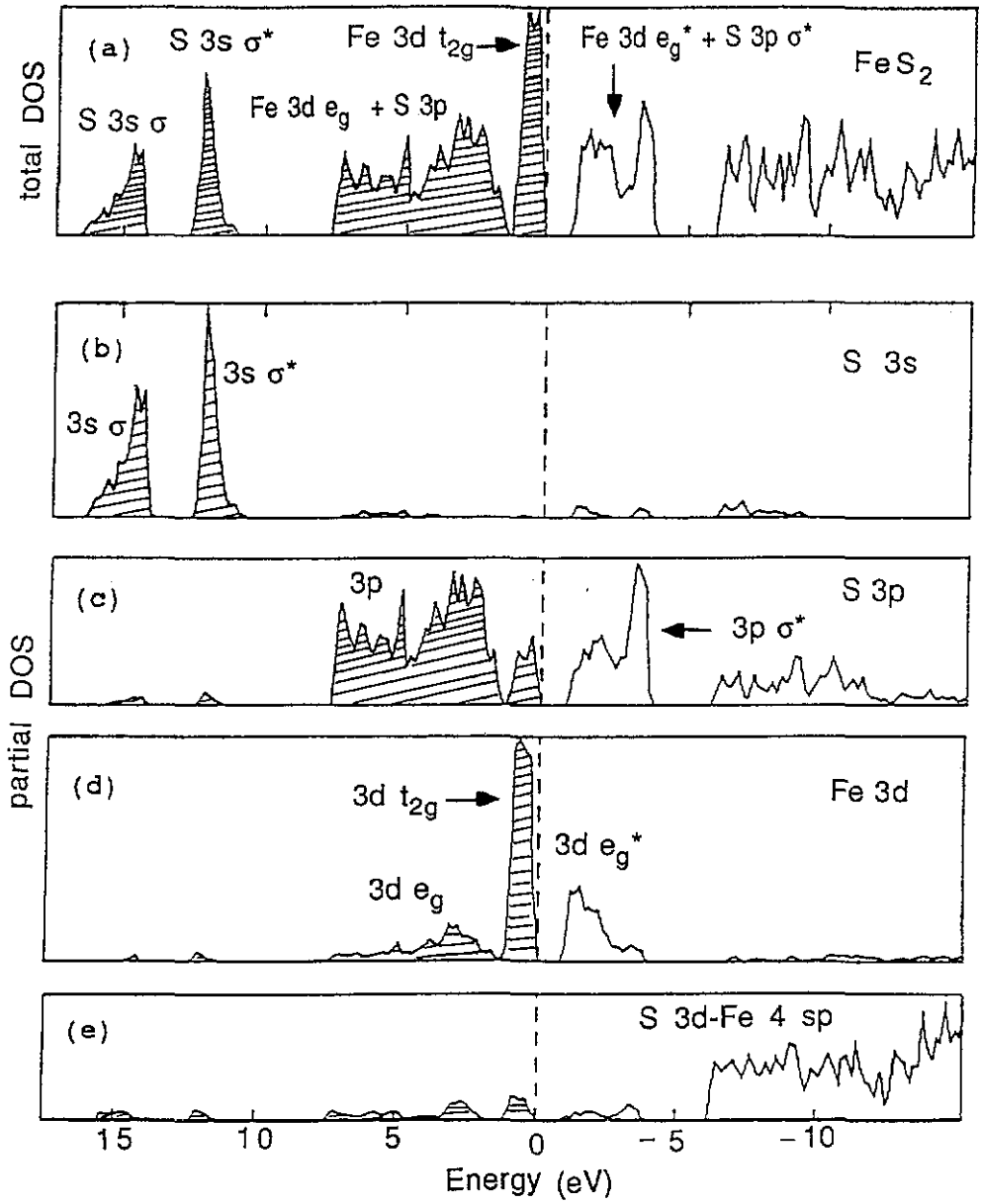

Figure 3. (a) The total DOS and (b)–(e) the partial DOSS of FeS_2 from [18]: (a) total DOS of FeS_2; (b) S 3s; (c) S 3p; (d) Fe 3d; (e) Fe 4sp–S 3d.

able to assign the indirect gap as the transition between the Fe 3d t_{2g} and S 3p σ^* states. Combining the results of the EER measurements and the recent report of the photoconduction of FeS_2 [30], we construct a possible energy band structure near the Fermi level. It is proposed that FeS_2 has a completely filled 3d t_{2g} band occupied by six electrons in the low-spin configuration, separated 0.83 eV from empty S 3p σ^* and Fe 3d e_g^* bands, and the bottom of the conduction band corresponds to the S 3p σ^* antibonding states. A band-

structure scheme consistent with the transition energies shown in table 1 is constructed in figure 4.

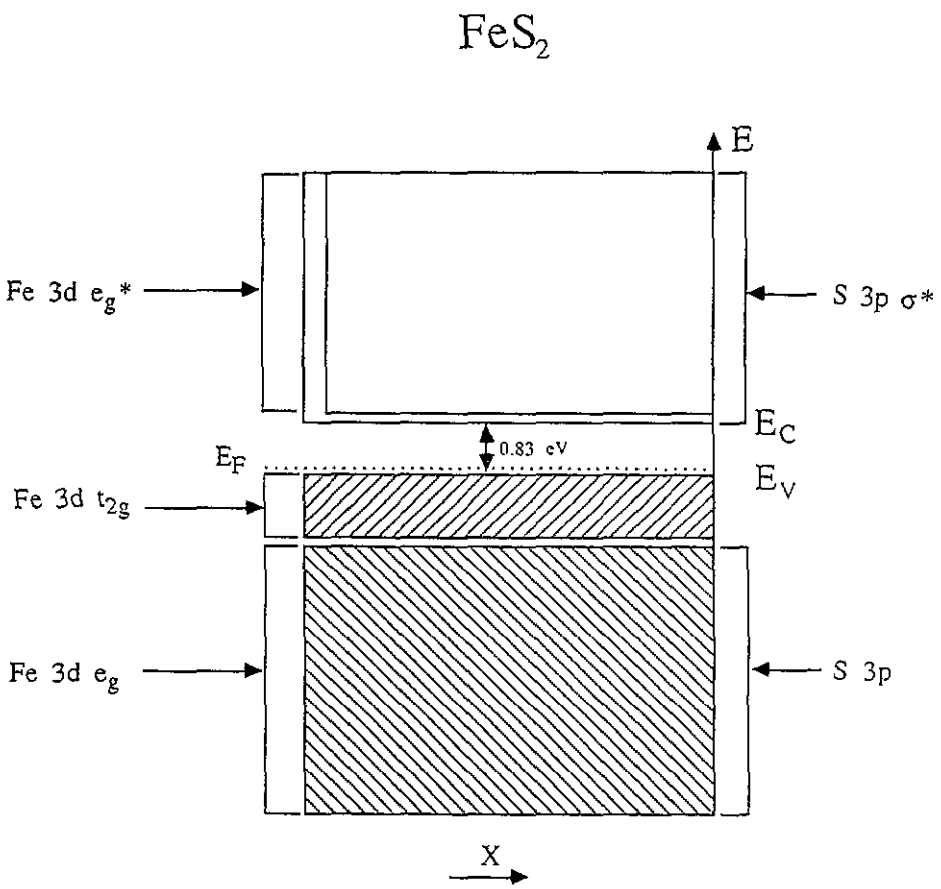

Figure 4. Energy level scheme near the Fermi level of FeS_2.

There is additional evidence to support our assignment. In the study of the photoelectrochemical evolution of oxygen with the FeS_2 electrode, we have observed that the FeS_2 crystal shows clear evidence of corrosion after photochemical oxidation by white light in 1 N H_2SO_4 for 10 h [34]. This result can be related to the fact that the excitations are from the Fe 3d t_{2g} to the S 3p σ^* antibonding molecular orbital, which tends to weaken the S–S bond in the pyrite structure, rather than the d–d transitions. Transition-metal dichalcogenides such as MoS_2 and WS_2, in which the lowest-energy interband transitions are primarily intra-atomic d–d transitions [35, 36], make stable photoelectrochemical electrodes. In these materials, in contrast with FeS_2, the photoelectrochemical reaction does not attack the metal–sulphur chemical bonds and therefore photocorrosion occurs less readily. The presence of an empty S 3p σ^* state near the Fermi level is very important in understanding the properties of pyrite. These states strongly hybridize with the Fe 3d states, giving rise to a large oscillator strength for virtual transitions from Fe 3d t_{2g} to S 3p σ^* at low frequencies ($h\nu \leqslant 1$ eV). This causes the large polarizability of FeS_2. The high-frequency dielectric

constant ϵ_∞ of FeS_2 is about 26 [23, 24], which is large indeed compared with values of, for instance, transition-metal iodides, $\epsilon_\infty = 5$–6 [37]. Such a highly polarizable environment means that local Coulomb interactions on the Fe atom are very much screened, resulting in a strongly reduced value for the effective Coulomb interaction between the 3d electrons of the Fe atom.

4. Conclusions

EER measurements have been carried for FeS_2 single crystals. The EER spectrum exhibits differential-like structures in the vicinity of the interband transitions. Thus a possible energy band structure near the Fermi level is constructed. It is proposed that FeS_2 has a completely Fe 3d t_{2g} band occupied by six electrons in the low-spin configuration, separated by 0.83 eV from the empty S 3p σ^* and Fe 3d e_g^* bands. The bottom of the conduction band corresponding to the S 3p σ^* antibonding states is very important in understanding the properties of pyrite.

Acknowledgment

The authors acknowledge the support of the National Science Council of the Republic of China.

References

[1] Jaegermann W and Tributsch H 1983 *J. Appl. Electrochem.* **13** 743
[2] Ennaoui A and Tributsch H 1984 *Solar Cells* **13** 197
[3] Lalvani S B and Shami M 1986 *J. Electrochem. Soc.* **133** 1364
[4] Vincent C A 1984 *Modern Batteries* (London: Arnold)
[5] Pemsler J M, Lam R K F, Litchfield J K, Dallek S, Larrick B F and Beard B C 1990 *J. Electrochem. Soc.* **137** 1
[6] Sato K 1985 *Prog. Cryst. Growth Characteristics* **11** 109
[7] Dunn J G, De G C and O'Connor D H 1989 *Thermochim. Acta* **145** 115
[8] Marinace J C 1954 *Phys. Rev.* **96** 593
[9] Bither T A, Bouchard R J, Cloud W H, Donohue P C and Siemons W J 1968 *Inorg. Chem.* **7** 2208
[10] Sasaki A 1955 *Miner. J. Japan* **1** 290
[11] Horita H and Suzuki T 1973 *J. Phys. Soc. Japan* **33** 1723
[12] Schlegel A and Wachter P 1976 *J. Phys. C: Solid State Phys.* **9** 3363
[13] Kou W W and Seehra M S 1978 *Phys. Rev.* B **18** 7062
[14] Pollak F H 1981 *Proc. Soc. Photo-Opt. Instrum. Eng., Proc. SPIE* vol 276 (Bellingham, WA: SPIE) p 142
[15] Aspnes D E 1980 *Handbook on Semiconductors* vol 2, ed M Balkanski (New York: North-Holland) p 109
[16] Macfarlane R M, Ushioda S and Blazey K W 1974 *Solid State Commun.* **14** 851
[17] Salvador P, Tafalla D, Tributsch H and Wetzel H 1991 *J. Electrochem. Soc.* **138** 3361
[18] Folkerts W, Sawatzky G A, Haas C, de Groot R A and Hillebrecht F U 1987 *J. Phys. C: Solid State Phys.* **20** 4135
[19] Lauer S, Trautwein A X and Harris F E 1984 *Phys. Rev.* B **29** 6774
[20] Bullett D W 1982 *J. Phys. C: Solid State Phys.* **15** 6163
[21] Ohsawa A, Yamanoto H and Watanabe H 1974 *J. Phys. Soc. Japan* **37** 568
[22] Li E K, Johnson K H, Eastman D E and Freeouf J L 1974 *Phys. Rev. Lett.* **32** 170
[23] Suga S, Inoue K, Taniquchi M, Shin S, Seki M, Sato K and Teranishi T 1983 *J. Phys. Soc. Japan* **52** 1848
[24] Sato K 1984 *J. Phys. Soc. Japan* **53** 1617
[25] Huang Y S and Chen Y F 1988 *Phys. Rev.* B **38** 7997
[26] Holzwarth N A W, Harris S and Liang K S 1985 *Phys. Rev.* B **32** 3745

[27] Huang Y S and Lin S S 1988 *Mater. Res. Bull.* **23** 277
[28] Yu J T, Wu C J, Huang Y S and Lin S S 1992 *J. Appl. Phys.* **71** 370
[29] Moss T S 1959 *Photoconductivity in the Elements* (London: Butterworth)
[30] Tsay M Y, Huang Y S and Chen Y F 1993 *J. Appl. Phys.* **74**
[31] Huang Y S, Chen H M, Chang C J and Jan G J 1985 *Chin. J. Phys.* **23** 144
[32] Aspnes D E 1973 *Surf. Sci.* **37** 418
[33] Ballhansen C J 1962 *Introduction to Ligand Field Theory* (New York: McGraw-Hill)
[34] Huang Y S and Chen Y F unpublished
[35] Tributsch H and Bennett J C 1977 *J. Electranal. Chem.* **81** 97
[36] Tributsch H 1982 *Struct. Bonding* **49** 127
[37] Pollini I, Thomas J, Jezequel G, Lemennier J C and Lenselink A 1984 *Phys. Rev.* B **29** 4716